ELSEVIER

Thermochimica Acta 282/283 (1996) 385–397

thermochimica acta

The emanation thermal analysis of kaolinite clay minerals[1]

V. Balek [a,*], M. Murat [b]

[a] *Nuclear Research Institut Řež, Cz-250 68 Řež, Czech Republic*

[b] *Institut National des Sciences Appliquées (INSA) de Lyon, Groupe d'Etudes de Métallurgie Physique et de Physique des Matériaux (G.E.M.P.P.M.), URA CNRS No 341, 20 av. Albert Einstein, F-69621, Villeurbanne Cedex, France*

Abstract

Emanation thermal analysis (ETA) is based on the measurement of the rate of release of radon from solid samples previously labelled with trace concentrations of an inert radioactive nuclide (Thorium-228 or Ra-224). This method enables pointing out of the different steps that occur during the heating of kaolinite: pre-dehydroxylation, dehydroxylation, evolution of structural disorder in metakaolinite, segregation of amorphous silica and formation of precursors of high-temperature phases, crystallization and sintering of both mullite and cristobalite. The investigations of two kaolinite samples of quite different crystallinity demonstrates the role of the structural disorder of the mineral in the manifestation of these structural changes. The differences observed between the behaviour of the two samples are reflected by different diffusivities of radon which can be related to different morphology changes taking place in kaolinite during heating. The results obtained demonstrate the potential of ETA as a complementary method of conventional thermoanalysis and XRD methods.

Keywords: Clay; Crystallinity; Emanation thermal analysis (ETA); Kaolinite; Radon release; Radiolabelled clay; Structural disorder

1. Introduction

A number of methods has been used in the characterization of the thermal behaviour of kaolinitic clay minerals [1], such as thermogravimetry [2], differential thermal analysis [3, 4], thermodilatometry [5, 6], IR spectroscopy [7], X-ray diffrac-

* Corresponding author.

[1] Dedicated to Takeo Ozawa on the Occasion of his 65th Birthday.

PII S0040-6031(96)02886-9

tometry, X-ray spectropscopy and the radial electron density distribution technique [8], and many other more sophisticated methods. In the present paper we want to demonstrate the potential of emanation thermal analysis (ETA) as a complementary method to conventional thermoanalysis (TG, DTA) and XRD analysis.

2. Experimental

2.1. Sample investigated

Two kaolinite samples of quite different crystallinity have been investigated, namely a very poorly crystallized sample (denoted FON) from the Font Bouillant quarry, AGS Co, Charentes, France, and a well crystallized kaolinite sample (denoted ANG) of English origin. Chemical compositions of both samples, determined by Vaucquelin [9] are given in Table 1 together with the values of the slope ratio, maesured by DTA in air, the Hinckley index [10], measured by XRD, the BET specific surface area measured by nitrogen adsorption, and the nature of the main impurities. The FON sample also contained some gel-like kaolinite, as mentioned by Liétard [11].

Scanning electron micrographs of the original kaolinite (Fig. 1) indicate that the texture of ANG sample consists of densely packed sheets [12] with more or less

Table 1
Chemical composition percent by weight and characteristics of the raw kaolinite samples (measured by Vaucquelin, [9])

Oxides	ANG	FON
SiO_2	47.53	43.20
Al_2O_3	35.68	34.53
Fe_2O_3	0.71	1.36
Na_2O	0.05	0.01
CaO	traces	0.01
MgO	0.26	0.08
K_2O	1.76	0.04
TiO_2	0.05	3.54
Weight loss at 1000°C/%	13.00	15.92
Total/%	99.04	98.69
Absorbed water/%	1.21	3.35
Spec. surf. area/(m^2g^{-1})	14.5/13.8	61.2/54[a]
Hinckley index	1.30[a]	0.70[a]/0.65[b]
DTA slope ratio[c]	1.55/1.62[a]	2.75/2.78[a]
Impurities	Muscovite, quartz	Anatase, iron oxide, quartz

[a] Measured by the authors.
[b] Measured by Liétard [11].
[c] Measured on the DTA endothermic dehydroxylation peak of kaolinite by the method of Mackenzie [4].

Fig. 1. Scanning electron micrographs of samples ANG (1) and FON (2).

dispersed stacked platelets, while that of the FON sample is more compact and consists of packed nodules of very small-sized platelets without any well-defined geometry.

The role of crystallinity of both samples was previously investigated after calcination of the clay at different temperatures, either with the aim of zeolite synthesis [13], or of invetigating the first step of the metakaolinite to mullite transition [14] and the nature and crystallinity of high-temperature phases (mullite and cristobalite) up to 1600°C [15].

2.2. *Emanation thermal analysis*

2.2.1. *Principle of the method*

Emanation thermal analysis (ETA) is based on the measurement of the release of the inert gas atoms (e.g. radon) from solid samples previously labelled with trace concentrations of inert radioactive gases or their parent nuclides [16–18]. The inert gases do not react with the solid and their release is controlled by the diffusion in the matrix, diffusion in pores and by the recoil energy which every atom of radon gains during its formation from its parent according to the scheme: Th-228 $-\alpha\rightarrow$ Ra-224 $-\alpha\rightarrow$ Rn-220 $-\alpha\rightarrow$ .....

The solids are labelled with the parent nuclide of radon by adsorption (from aqueous or non-aqueous solution) on their surface, the radon atoms introduced by the recoil energy of the spontaneous alpha decay (100 ke V atom^{-1} penetrate to a maximum depth of 80 nm from the surface.

The release of the radon atoms from a solid is controlled by the recoil of radon atoms as well as by radon diffusion in pores and in the matrix. According to theoretical considerations [16, 18] the rate of the radon release (E) from a sample can be expressed in a simplified form as follows:

$$E = S[K_1 + K_2(D/\lambda)^{1/2}] \tag{1}$$

where S is the surface area of the sample, K_1 is a temperature-independent constant expressing the recoil path of the radon in the material, K_2 is a temperature-dependent constant, D is the coefficient of radon diffusion in the sample, and λ is the randon decay constant.

From eq. (1) it follows that any process in a solid or its phase boundary leading to a change in either surface and/or changes in radon diffusivity (permeability) becomes indirectly observable from the ETA measurements. An increase in the radon release rate indicates an increase in the mineral surface area, the loosening of the structure and fabric and the appearance of other irregularities, resulting, e.g., from the decomposition or phase transformations taking place in the mineral layers labelled with the radon. A decrease in the radon release rate indicates a decrease in the mineral surface area, annealing of surface defects, compaction of the fabric and micro-structure of the sample resulting, e.g., from sintering of the samples.

On the other hand, ETA can be recommended for the characterization of highly porous solids, mainly containing micropores. This method is especially sensitive to changes in the microporosity, as the pore size of the micropores is compatible with the diameter of radon atoms (0.38 nm).

ETA results are considered as complementary information to the characterization of the thermal behaviour of minerals. They are usually compared with results of traditional thermal analysis methods (such as DTA, TG), XRD and surface area measurements.

2.2.2. Procedures

The ETA device used in this paper was constructed at the Nuclear Research Institute Rez and was based on Netzsch 409 DTA equipment. The kaolinite samples were heated at a rate of 5 K min^{-1} in air flowing at 40 mL min^{-1}. The samples were previously labelled with Th-228 and Ra-224 by adsorption from acetone solution (specific radioactivity of the sloution 10.5 Bq), and dried at room temperature and pressure. The amount of sample used for the ETA measurement was 0.1 g. The results of the ETA are presented as the dependences in temperature of the radon release rate E, where E represents the radon activity released from the sample normalized to the total radioactivity of the parent nuclides absorbed on the sample surface by labelling.

2.3. Other methods used as comparison

Samples were previously investigated by traditional methods of thermal analysis:

(1) TG–DTA (TG–DTA 92 Setaram device; sample weight, 0.025 g; heating rate, 5 K min^{-1}; atmosphere, helium);

(2) DSC (AF DSC Setaram apparatus; sample weight, 0.2 g; heating rate, 5 K min^{-1}; atmosphere argon.

XRD identification (powder pattern) of the kaolinite samples calcined for 3 h in static air from 800°C to 1260°C, then cooled at ambient temperature, was performed with a Siemens D 500 diffractometer with CuK_{α} radiation.

BET specific surface area of samples fired up to 1100°C, also used for interpretation of ETA results, was measured using nitrogen adsorption volumetry at 77 K in a Carlo Erba apparatus.

3. Results and discussion

Before discussing ETA results, we must recall the main structural changes pointed out by TG, DTA or DSC during heating of kaolinite to 1300°C:

(1) *Step No. 1*: low-temperature release of absorbed water ($T \leq 100$°C);

(2) *Step No. 2*: dehydroxylation in the temperature range 400–500°C

Steps 1 and 2 both give rise to endothermic peaks on the DTA curve and to loss of weight on TG curves.

(3) *Step No. 3*: Release of residual hydroxyl groups of metakaolinite with segregation of alumina and silica, not detectable on the DTA curve, but giving rise to a continuous slight loss of weight on the TG curve up to 900–1000°C

(4) *Step No. 4*: Formation of 'precursors' (γ-alumina, amorphous silicate, nuclei of 'primary mullite', etc...) of high-temperature phases (mullite and cristobalite) producing the sharp exothermic peak at about 980°C on the DTA curve;

(5) *Step No. 5*: Crystallization of mullite and/or cristobalite giving rise to exothermic peaks of low or middle intensity of the DTA curve above 1100°C.

No specific weight loss occurs during steps 4 and 5.

On the other hand, the temperature of the onset of the dehydroxylation endothermic peak (Step No. 2) is noticeably lower for a poorly-crystallized kaolinite [19–21]. The same phenomenon occurs for the sharp exothermic peak around 980°C (Table 2) and the stability range of precursors of high temperature phases is higher [14].

ETA curves of the investigated kaolinite samples are given in Fig. 2 (ANG sample: curve 1; FON sample: curve 2). The results of the TG and DTA obtained from the simultaneous measurements are given in Figs. 3 and 4 for the well crystallized kaolinite

Table 2
T_0/T_m value couple (T_0 *and* T_m temperature at the onset and the maximum of the DTA peak, respectively) for samples ANG and FON

	Dehydrox.	Dehydrox.	Exo 980°C	Exo 980°C	Exo 980°C
Sample	Air[a]	Helium	Air[a]	Helium	Argon
ANG	409/594	400/508	958/976	962/988	968/997
FON	358/586	350/493	925/958	937/970	952/984

[a] DTA in air on 1.5 g; heating rate, 2 K min^{-1} (curve not given in the paper).

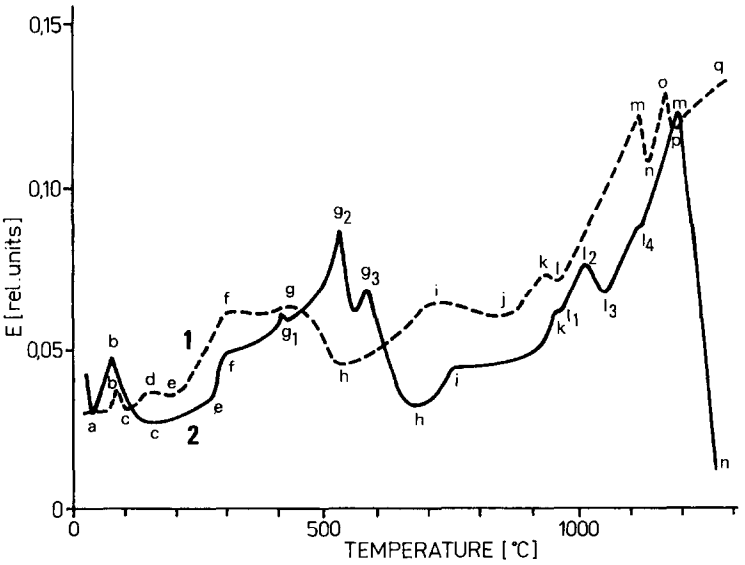

Fig. 2. ETA in air, of kaolinite samples ANG (curve 1) and FON (curve 2).

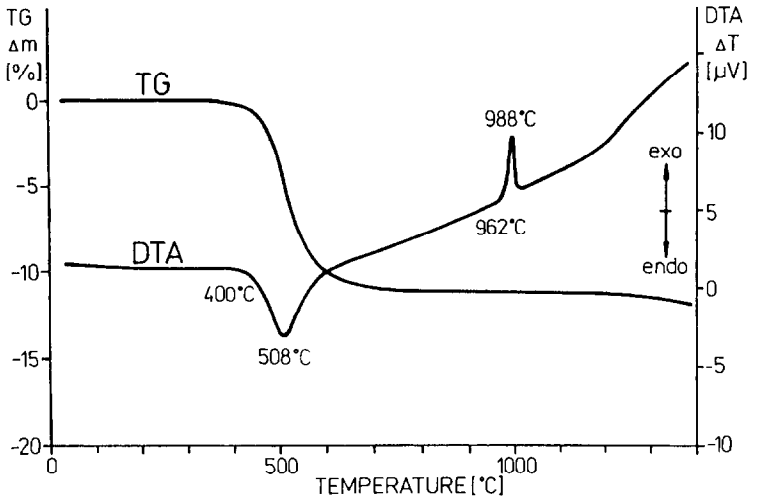

Fig. 3. TG and DTA curves of kaolinite sample ANG (helium atmosphere).

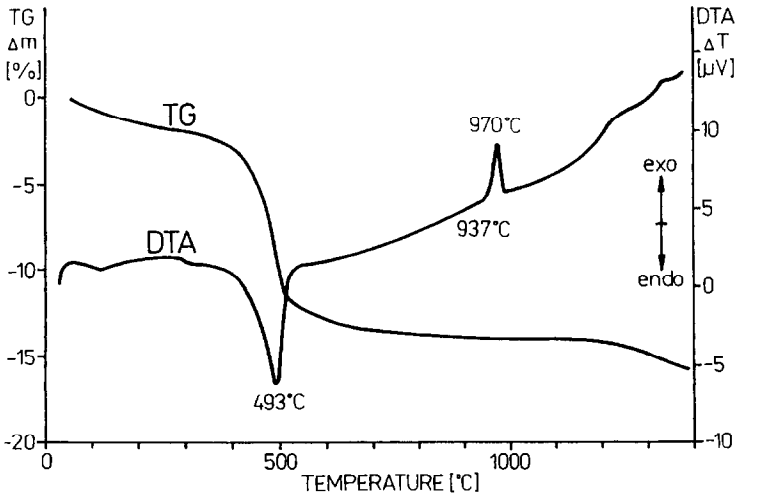

Fig. 4. TG and DTA curves of kaolinite sample FON (helium atmosphere).

sample (ANG) and for the poorly crystallized sample (FON), respectively. The evolution of both the nature of phases formed (XRD identification) and the variation of the specific surface area after the firing of the kaolinite samples from 800°C to 1260°C is given in Table 3.

Table 3
Evolution of BET specific surface area and of the nature of phases according to the firing temperature of both kaolinite samples for 3 h in air. The dotted line indicates the limit of firing temperature for which the exothermic peak at 980°C disappears on the DTA curve of th fired sample

	ANG		FON	
T/°C	S/(m^2 g^{-1})	XRD	XRD	S/(m^2 g^{-1})
25	13.8	Kaolinite	Kaolinite	54
800	13.4	Am	Am	53
850	12.2	Am	Am	51.3
900	11.1	Am	Am + γ-A(w)	42.3
1000	8.3	Am + M(w) + γ-A(m)	Am + γ-A(m)	37.0
1100	6.5	Am + M(m) + γ-A(m)	Am + M(vw) + γ-A(w)	23.0
1260	–	Am + M(s) + Cr(w)	Am + M(s) + Cr(s)	–

Am: amorphous background; γ-A: γ-alumina; M: Mullite; Cr: cristobalite.
(vw), (w), (m), (s): very weak, weak, middle and strong intensity, respectively.

3.1. *ETA results from the well crystallized sample (ANG)*

The radon release rate, E, (Fig. 2, curve 1) shows differents events.

(1) A peak **abc,** of low intensity, that reflects the release of absorbed water; this phenomenon can differ from one sample to another according to the drying conditions of samples after labelling.

(2) An increase in E from 160°C to 300°C (part **cdef** of the curve); this can be correlated with the *pre-dehydroxylation* process which, according Fripiat and Toussain [22], takes place on heating the kaolinite prior to dehydroxylation at the temperature 100–360°C. In this temperature interval the increase in the radon release indicates some reorganization process in the kaolinite crystals. According to Fripiat and Toussaint, some protons are delocalized as the result of the reorganization in the octahedral layer, as they observed by conductimetric measurements and infrared spectroscopy. It is worth mentioning that ETA makes it possible to reveal such structural changes. The mobility of radon atoms is strongly influenced by the fine changes in the structure units and interlamella space of kaolinite crystals. This results can be correlated with the findings do Freund [23] who pointed out that, with rising temperature, proton transfer associated with the predehydroxylation process occurs first *at the surface*, since the amplitudes of OH bendings are larger there than inside the crystal.

(3) A decrease **gh** of the radon release rate between 440°C and 530°C corresponds to the DTA peak of dehydroxylation of kaolinite (Fig. 3) with release of water molecules and formation of metakaolinite, according to the chemical reaction:

$$\underset{\text{(kaolinite)}}{Si_2O_5Al_2(OH)_4} \rightarrow \underset{\text{(metakaolinite)}}{Si_2O_5Al_2O_{2-x}(OH)_x} + \underset{\text{(water vapour)}}{(2-x/2)H_2O}$$

with a low value of x (about 10% of residual hydroxyl groups in metakaolinite, [24]).

This decrease **gh** of E reflects:

(i) either the arrangement of metakaolinite into 'pseudo-sheets' as a result of the combination of two successive dehydroxylated sheets to form more stable entities responsible for TEM fringes of 10–13 Å, recently observed by Dion [21], with creation of a nanometric tridimensional porosity in the structure of metakaolinite;

ii) or the formation of porous platelet agglomerates, indicated by a sensitive decrease in the external surface with no detectable decrease of the total BET surface, as demonstrated recently by Garcia-Diaz [25]. Effectively, the BET surface area measured by nitrogen adsorption did not change for samples heated up to 800°C (Table 3).

(4) From 350°C to 720°C, a new increase **hi** in E with a maximum at point **i**; this can be interpreted in terms of establishment of the maximum structural disorder of metakaolinite, a phenomenon that was pointed out using other experimental techniques [26–29];

(5) From 720°C to 850°C, the small decrease **ij** in E can be correlated with the onset of the 'recrystallization' or 'sintering of metakaolinite [21], or to the collapse of the metakaolinite pseudo-lattice giving way to extensive segregation of alumina and silica [30]. It corresponds to the onset of the decrease in the BET specific surface area of the sample (Table 3).

(6) Between 850°C and 940°C, the new increase in E (part **jk** of the curve) followed by a small decrease in E above 940°C occurs (part **kl**): this latter behaviour corresponds to the manifestation of the sharp exothermic DTA peak (Fig. 3) that reflects the formation of the precursors of high-temperature phases. According to different authors, the nature of these precursors can be different, such as: amorphous silica + cubic Al–Si spinel [31] or γ-alumina [7] with or without an amorphous aluminosilicate phase [8, 30, 32], 'primary mullite' [33] or 'cubic mullite' [34]. More recently Sanz et al. [35] suggested that the interpretation of the exotherm of kaolinite at 980°C must be interpreted in terms of a modification of the coordination of aluminium rather than a crystallization process, in agreement with the poor crystallinity of the high-temperature precursors identified on XRD patterns of samples fired isothermally in the temperature range 900–1100°C (Table 3): for isothermal firing of sample ANG at 1000°C, the XRD analysis indicates the presence of an amorphous phase + a minute content of poorly crystalline γ-alumina and 'primary mullite'. The formation of poorly crystallized γ-alumina and primary mullite phases is effectively reflected by a decrease in E, due to the higher density of γ-alumina ($d = 3.5$) and mullite ($d = 3.1$) compared with metakaolinite ($d = 2.6$) and amorphous silica ($d = 2.2$) [30].

(7) Above 960°C, a new increase in E is observed with two peaks at point **m** (1120°C) and point **o** (1170°C): the increase **lm** is associated with the heat-enchanced diffusion of radon which is disturbed at points **m** and **o** by the crystallization of mullite and cristobalite, as confirmed by high-temperature DTA results (Table 3 and [15]) curve 1, exothermic peaks with maxima at 1142°C and 1203°C, respectively);

(8) The new increase **pq** in E up to 1300°C corresponds to the heat-enhanced diffusion of radon associated with the onset of a limited sintering of high-temperature phases.

3.2. ETA results of the poorly crystallized sample (FON)

Some differences can be observed of the ETA curve of the FON sample (Fig. 2, curve 2).

(1) The intensity of the **abc** peak of the radon release rate, which reflects the release of absorbed water, is measureably higher, owing to the higher content of absorbed water, as indicated by the TG and DTA curves (Fig. 4).

(2) The onset (point **c**) of the radon release rate increase for the poorly crystallized FON sample takes place at lower temperature (160°C) than for the well crystallized ANG sample (200°C).

(3) In the temperature interval 350–540°C, that corresponds to dehydroxylation of kaolinite (endothermic peak on the DTA curve, Fig. 4) and where a decrease **gh** of E was expected on the ETA curve, an increase of the radon release rate with three radon bursts ($\mathbf{g}_1$, $\mathbf{g}_2$ and $\mathbf{g}_3$) was observed instead. The changes of radon release rate correspond to the complex behaviour of the FON sample in this temperature interval, as the sample is poorly crystallized and contains of gel-like kaolinite [11]. The more intense burst of radon $\mathbf{g}_2$, taking place below 500°C, may be ascribed to the opening of micropores in the gel-like kaolinite as a result of the release of water formed during the dehydroxylation process. A similar phenomenon was observed by one of us when characterizing the thermal behaviour of silica gel [36]. But this hypothesis does not hold because of gel of kaolinite would be transformed into metakaolinite at lower temperature than would a crystal of kaolinite. A more plausible hypothesis could be that it is a manifestation of *metakaolinite organization* as the kaolinite sample was poorly crystallized: this phenomenon can be decomposed into two or three steps due to the presence of gel-like kaolinite in the original sample, the less intense $\mathbf{g}_1$ burst reflecting, for example, the behaviour of the gel-like kaolinite, the $\mathbf{g}_2$ and $\mathbf{g}_3$ bursts of the poorly-crystalline FON sample are, perhaps, independent of the content of the gel-like phase, the sample being a mixture of two kaolinites of different crystallinity. Effectively, due to the Hinckley index value (0.65–0.70), the FON sample may be considered as a mixture of two kaolinites: one almost free from defects, the other richer in defects [37]. These manifestations of radon bursts during dehydroxylation of kaolinite may also be due to the particular compact texture of the sample. But all these assessments need complementary investigations on a larger series of kaolinite samples, the investigations reported in this paper concern the behaviour of two kaolinite because samples at the extremes of crystallinity.

(4) On further heating, the increased opened microporosity of the kaolinite collapsed. This process is reflected by the decrease after points $\mathbf{g}_2$ and $\mathbf{g}_3$ of the radon release rate above 500°C. The subsequent decrease in E observed on curve 2, Fig. 2, is deeper and corresponds to the annealing of the active surface of the sample and the formation of poorly crystalline metakaolinite with establishment of the double-sheet entities associated with the creation of the nanometric tridimensional porosity [21] and the agglomeration to the metakaolinite platelets [25], all phenomena that can be enhanced with a kaolinite sample characterized by high specific BET surface area and poor crystallinity.

(5) The new increase **hi** in E from 645°C to 750°C reflects the increase in the structural disorder in metakaolinite.

(6) No decrease **ij** observed on the ETA curve between 720°C and 850°C: this behaviour might be associated with segregation of a larger quantity of amorphous silica (density 2.2 against 2.6 for metakaolinite), a phenomenon that was previously observed with the FON sample [14]. It was also pointed out that the rate of 'recrystallization' or of 'sintering' of metakalonite above 750°C is measurably lower with the FON sample [28].

(7) The two discontinuities in E ($\mathbf{kl}_1$ and $\mathbf{l}_2\mathbf{l}_3$ at 960°C and between 1020°C and 1055°C, respectively) correspond to the formation of poorly crystallized γ-alumina. The formation of mullite nuclei occurs only at 1100°C (Table 3) and corresponds to the small discontinuity in the ETA curve at point $\mathbf{l}_4$, a discontinuity which occurs during the heat-induced diffusion of radon in the material (part $\mathbf{l}_3\mathbf{p}$ of the curve). ETA curves thus enable confirmation that the temperature interval of stability of the precursors of high-temperature phases is larger for the poorly crystallized kaolinite FON sample than for the well crystallized ANG samples: nucleation of 'primary mullite' from the ANG sample takes place in the temperature interval 950–975°C, whereas it is shifted by more than 100°C towards higher temperatures with the poorly crystallized FON sample.

(8) The sudden decrease **pn** of the radon release rate at temperature above 1190°C is related to both phenomena: the crystallization of mullite + cristobalite (XRD results in Table 3 and the exothermic DTA peak with a maximum at 1233°C [15]) and the immediate sintering of these high-temperature phases. The first pnenomenon demonstrates that the lower crystallinity of the kaolinite sample, the higher the thermal stability of the presursors of high temperature phases, as previously observed by Lemaître et al [30], Bulens and Dulmon [38] and Murat et al. [14]. We suppose that the high densification observed with FON sample, reflected on the ETA curve by the sharp decrease of the radon release rate, can result from the synergistic effect of the simultaneous formation of mullite and cristobalite in the same temperature interval, with probable formation of a surface glassy coat promoted by the impurities (iron and titanium oxides) contained in the original kaolinite sample.

4. Conclusion

We have demonstrated that emanation thermal analysis gives information supplementary to that obtained by the traditional methods, TG and DTA, used for characterization of kaolinite clays. Differences in the behaviour of the kaolinitic clay samples with different crystallinity were indicated by means of ETA during heating of the samples. The differences observed are based on different diffusivities of radon in the samples measured at elevated temperatures as well as on the different morphology and structure changes.

The results presented in this paper demonstrate that the ETA curves can be used as fingerprints of kaolinitic clay samples of different crystallinity and morphology.

In the coming work we shall demonstrate how the emanation thermal analysis reflects changes in the morphology and crystallinity of kaolinitic clay caused by weathering and interactions of the clay with water in the environment.

Acknowledgements

Part of the experimental work was carried out within the terms of research grant No. 205-93-0701 awarded by the Grant Agency of the Czech Republic. The authors wish to express their gratitude to the Grant Agency of the Czech Republic for the financial support.

Many thanks are due to Mrs E. Klosová, Nuclear Research Institute Řež for the ETA measurements and to Dr F. Sorrentino, Lafarge Coppée Recherche, France for SEM microphotographs of the kaolinite samples.

References

[1] G.W. Brindley and J. Lemaitre, Thermal Oxidation and Reduction Reactions of Clay Minerals, in A.C.D. Newman (Ed.), Chemistry of Clays and Clay Minerals, Longman Scientific and Technical, Mineralogical Society, 1987, pp. 319–370.
[2] G. Liptay G. (Ed.), Atlas of Thermoanalytical Curves, Vol. 1, Heyden and Son Ltd, 1971, p. 37.
[3] R.C. Mackenzie, The Differential Thermal Analysis of Clays, Mineralogical Society, London, 1957.
[4] R.C. Mackenzie, Differential Thermal Analysis, Academic Press, London and New York, 1970.
[5] C. Kiefer, Bull. Soc. Fr. Céram., 35 (1957) 95–114.
[6] A.K. Chakraborty, J. Am. Ceram. Soc., 75 (1992) 2013–2016.
[7] H.J. Percival, J.F. Duncan and P.K. Foster, J. Am. Ceram. Soc., 57 (1974) 57–61.
[8] A.J. Leonard, J. Am. Ceram. Soc., 60 (1977) 37–43.
[9] M. Vaucquelin, Ph. D. Thesis, University of Limoges, 1980.
[10] D.N. Hinckley, Proc. 11th Nat. Conf. Clays and Clay Miner., Pergamon Press, Oxford, 1963, pp. 229–235.
[11] O. Lietard, Ph. D. Thesis, University of Nancy, 1977.
[12] J. Esteoule-Choux, Clay Miner., 16 (1981) 279–288.
[13] M. Murat, A. Amokrane, J.P. Bastide and L. Montanaro, Clay Miner., 27 (1992) 119–130.
[14] M. Murat, A. Amokrane, L. Montanaro and A. Negro, C.R. Acad. Sci., Paris. 316, Sér. II (1993) 907–912.
[15] J. Dubois, M. Murat, X. Carbonneau, A. Amroune and R. Gardon, Appl. Clay Sci., in press.
[16] V. Balek and J. Tölgyessy, Emanation Thermal Analysis and other Radiometric Emanation Methods. Akademiai Kiado, Budapest, and Elsevier, Amsterdam, 1984.
[17] V. Balek, J. Therm. Anal., 20 (1981) 495–518.
[18] V. Balek, Emanation Thermal Analysis and its Applications. Thermochim. Acta, 192 (1991) 1–17.
[19] M. Murat and A. Negro, Geolog. Applic. e Hydrogeol. Bari (Ital.) XII (II), (1977) 79–87.
[20] S.A.T. Redfern, Clay Miner., 22 (1987) 447–456.
[21] P. Dion, Ph. D. Thesis, University of Orléans, 1994.
[22] J.J. Fripiat and F. Toussaint, J. Phys. Chem., 67 (1963) 30–36.
[23] F. Freund, Proc. Int. Clay Conf., Tokyo, Vol. 1, Israel University Press, Jerusalem, 1969, Vol. 1, pp. 121–128.
[24] J.D. MacKenzie, I.W.M. Brown, R.H. Meinhold and M.E. Bowden, J. Am. Ceram. Soc., 68 (1985) 293–297.
[25] E. Garcia-diaz, Ph. D. Thesis, School of Mines d'Alès, 1995.
[26] A. Bachiorrini and M. Murat, Comptes-Rendus Acad. Sci., Paris, 303, Sér. II (1986) 1783–1786.

[27] M. Murat and M. Driouche, Clay Miner., 23 (1988) 55–56.
[28] M. Murat, Mathurin D. and M. El M. Chbihi M, Thermochim. Acta, 122 (1987) 79–85.
[29] M. Murat. D. Mathurin, M. Driouche, L. Montanaro and A. Bachiorrini, Sci. Géol. Bull. (Strasbourg), 43 (1990) 213–223.
[30] J. Lemaitre, A.J. Leonard and B. Delmon, Proc. Int. Clay Conf., Mexico City, Applied Publishing Ltd, Wilmette, Il, 1975, pp. 545–552.
[31] G.W. Brindley and M. Nakahira, J. Am. Ceram. Soc., 42 (1959) 319–324.
[32] J. Lemaitre, A.J. Leonard and B. Delmon B, Bull. Miner., 105 (1982) 501–507.
[33] H.D. Glass, Am. Miner., 39 [3/4] (1954) 193–207.
[34] A.K. Chakravorty, J. Am. Ceram. Soc., 62 (1979) 120–125.
[35] J. Sanz, A. Madani, J.M. Serratosa, J.S. Moya and S.ASA, J. Am. Ceram. Soc., 71 (1988) C-418–C-421.
[36] V. Balek V. and I.N. Beckman, Thermochim. Acta, 85 (1985) 15–18.
[37] A. Plancon, R.F. Giese Jr, R. Snyder, V.A. Drits and A.S. Bookin, Clays and Clay Miner., 25 (1989) 203–210.
[38] M. Bulens and B. Delmon, Clays Clay Miner., 25 (1977) 271–277.